ORBIT DETERMINATION ERROR ANALYSIS AND COMPARISON OF STATION-KEEPING COSTS FOR LISSAJOUS AND HALO-TYPE LIBRATION POINT ORBITS AND SENSITIVITY ANALYSIS USING EXPERIMENTAL DESIGN TECHNIQUES

Lieutenant Colonel Steven C. Gordon[†]

N93-24721

ABSTRACT

Spacecraft in orbit near libration point L1 in the Sun-Earth system are excellent platforms for research concerning solar effects on the terrestrial environment. One spacecraft mission launched in 1978 used an L1 orbit for nearly 4 years, and future L1 orbital missions are also being planned. Orbit determination and station-keeping are, however, required for these orbits. In particular, orbit determination error analysis may be used to compute the state uncertainty after a predetermined tracking period; the predicted state uncertainty levels then will impact the control costs computed in station-keeping simulations. Error sources, such as solar radiation pressure and planetary mass uncertainties, are also incorporated. For future missions, there may be some flexibility in the type and size of the spacecraft's nominal trajectory, but different orbits may produce varying error analysis and station-keeping results. The nominal path, for instance, can be (nearly) periodic or distinctly quasi-periodic. A periodic "halo" orbit may be constructed to be significantly larger than a quasi-periodic "Lissajous" path; both may meet mission requirements, but perhaps the required control costs for these orbits are provably different. Also for this spacecraft tracking and control simulation problem, experimental design methods can be used to determine the most significant uncertainties. That is, these methods can determine the error sources in the tracking and control problem that most impact the control cost (output); it also produces an equation that gives the approximate functional relationship between the error inputs and the output.

INTRODUCTION

In one formulation of the problem of three bodies, when the mass of one of the bodies is sufficiently small (infinitesimal) so that it does not affect the motion of the other two bodies (primaries), the "restricted three-body problem" results. Five libration (Lagrange) points can be found as particular solutions of the equations of motion governing the path of the infinitesimal mass moving within the gravitational fields of the primaries. These equilibrium points are defined relative to a coordinate system rotating with the primaries. One Lagrange point, L1, is located between the primaries and is the libration point of interest here.

Three-dimensional, periodic and quasi-periodic orbits are currently being studied for upcoming missions. Periodic "halo" orbits in the vicinity of libration points have been studied since the late 1960s. Robert Farquhar coined the term "halo" to describe a three-dimensional, periodic orbit near a libration point on the far side of the Moon in the Earth-Moon system.[1] These orbits were designed to be large enough so that the spacecraft would be constantly in view of the Earth and thus would appear as a halo around the Moon. Alternatively, the variations in size and shape that a quasi-periodic orbit can exhibit may add

valuable flexibility for mission planning. This type of bounded, three-dimensional libration point trajectory is called a "Lissajous" orbit since specific planar projections of these quasi-periodic trajectories may look like a special type of Lissajous curve.

Howell and Pernicka[2] have developed a numerical technique for determination of three-dimensional, bounded libration point trajectories of arbitrary size and duration. Their numerical algorithm uses an analytic solution as a first approximation and then constructs a trajectory continuous in position and velocity. Their method is used in this study to define nominal paths in the Sun-Earth+Moon problem. The notation "Earth+Moon" means that the Earth plus the Moon are treated as one body with mass center at the Earth-Moon barycenter. The numerical data is then curve fit using a cubic spline routine, although the use of other curve fit methods[3] is possible. The assumed dynamic model is the elliptic restricted three-body problem (ER3BP), where the primaries move on known elliptic paths. The force model used here includes solar radiation pressure[4], the gravitational attractions of the Sun and the Earth+Moon barycenter, and the centrifugal force associated with rotation of the system.

The forces affecting the spacecraft orbit have differing levels of uncertainty, and, unfortunately, the spacecraft will drift from the nominal path. Both range and range-rate tracking also include inaccuracy in measurement. The accumulated error in the spacecraft's position and velocity relative to the nominal path after a predetermined period of tracking can be computed. This error, or uncertainty, in the spacecraft state is measured through simulations, commonly referred to as orbit determination error analysis, and is presented as a vector of standard deviations of the states. In this work, the state vector includes three position and three velocity states. The state uncertainty computed in the error analysis can then be input to a station-keeping algorithm that computes control manuevers to return the spacecraft to the vicinity of the nominal path. The algorithms incorporate certain minimal constraints for time between manuevers, control magnitude, and distance from the nominal path before a control manuever is input. For these algorithms, variations in orbital shapes and sizes may have some effect on the station-keeping costs.

BACKGROUND

Coordinate Systems

The coordinate systems used in this analysis have a common origin at the primaries' center of mass. Primaries with masses m_1 and m_2 such that $m_1 \geq m_2$ are assumed here. The infinitesimal mass is denoted as m_3. These masses (m_1, m_2, m_3) correspond to particles situated at points P_1, P_2, and P_3, respectively. The barycenter is denoted as "B," and the resulting arrangement is shown in Fig. 1. The rotating coordinate system is defined as $X_R Y_R Z_R$, and the inertial system is identified as $X_I Y_I Z_I$.
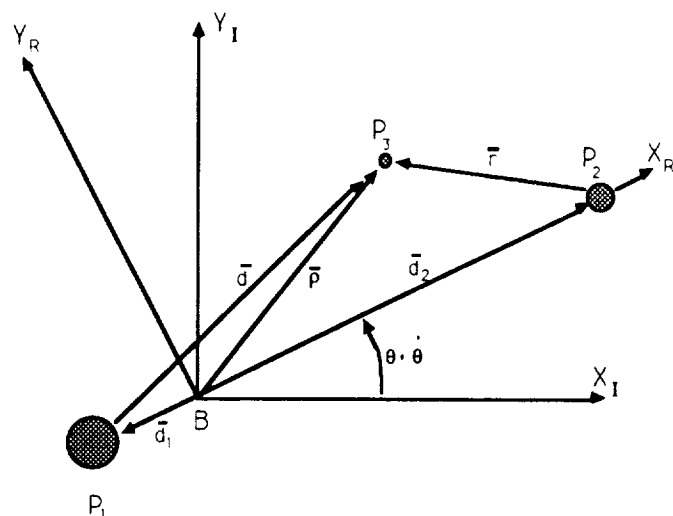
Fig. 1   Coordinate Systems Used

Note that both coordinate systems are right-handed, and the X and Y axes for both systems are in the plane of motion of the primaries. The rotating X_R axis is defined along the line that joins the primaries and is directed from the larger toward the smaller primary.

Equations of Motion

The equations of motion for m_3 (the spacecraft) relative to B as observed in the inertial reference frame are now formulated. The sum of the forces on m_3 resulting from both the gravity fields of masses m_1 (the Sun) and m_2 (the Earth-Moon barycenter) and from the solar radiation pressure can be used to produce the following second-order vector differential equation:

$$\bar{\rho}'' = - G \left(\frac{m_1}{d^3}\right) \bar{d} - G \left(\frac{m_2}{r^3}\right) \bar{r} + \left(\frac{kS}{d^3}\right) \bar{d}. \tag{1}$$

The overbar denotes a vector, and primes indicate differentiation with respect to dimensional time. All quantities are dimensional, as appropriate, and the quantity "G" is the universal gravitiational constant. The scalars "d" and "r" in Eq. (1) denote the magnitudes of vectors $\bar{d}$ and $\bar{r}$, respectively, depicted in Fig. 1. The dimensionless scalar "k" is the solar reflectivity constant, and "S" is the solar radiation pressure constant[5]. The position vector $\bar{\rho}$ is written in rotating components as

$$\bar{\rho} = x \, \hat{X}_R + y \, \hat{Y}_R + z \, \hat{Z}_R \tag{2}$$

where $\hat{X}_R, \hat{Y}_R, \hat{Z}_R$ are unit vectors. The kinematic expression for $\bar{\rho}''$ is:

$$\bar{\rho}'' = (x'' - \theta'' y - 2\theta' y' - \theta'^2 x) \, \hat{X}_R + (y'' + \theta'' x + 2\theta' x' - \theta'^2 y) \, \hat{Y}_R + z'' \, \hat{Z}_R. \tag{3}$$

Three scaled equations of motion for P_3 can be derived using the following definitions: the sum of the primary masses is one mass unit, the mean distance between the primaries is one distance unit, and the universal gravitational constant is equal to one unit by proper choice of characteristic time. The equations of motion can then be simplified and scaled by also introducing the nondimensional mass ratio μ, "psuedo-potential" U, and the scaled solar radiation constant s:

$$\mu = \frac{m_2}{m_1 + m_2} \tag{4}$$

$$U = \frac{(1-\mu)}{d} + \frac{\mu}{r} + \frac{1}{2} \dot{\theta}^2 (x^2 + y^2) - \frac{k \, s}{d} \tag{5}$$

where the dot denotes the derivative with respect to characteristic time. Then the vector magnitudes, "d" and "r," are written in terms of scaled quantities as:

$$d = [(x + \mu R)^2 + y^2 + z^2]^{1/2}, \tag{6}$$

$$r = [(x - R + \mu R)^2 + y^2 + z^2]^{1/2}. \tag{7}$$

The three second-order differential equations that result can be written in terms of characteristic (scaled) quantities as

$$\ddot{x} - 2 \dot{\theta} \dot{y} = \frac{\partial U}{\partial x} + \ddot{\theta} y = U_x + \ddot{\theta} y, \tag{8}$$

$$\ddot{y} + 2 \dot{\theta} \dot{x} = \frac{\partial U}{\partial y} - \ddot{\theta} x = U_y - \ddot{\theta} x, \tag{9}$$

$$\ddot{z} = \frac{\partial U}{\partial z} = U_z. \tag{10}$$

These three equations can then be used to propagate the spacecraft state forward in both the error analysis and station-keeping simulations.

Reference Paths Generated for This Work

In the ER3BP, precisely periodic halo orbits exist, but nearly periodic orbits are more practical and likely to be used in mission planning. Therefore, the goal here will be to compare results for quasi-periodic Lissajous and nearly periodic "halo-type" orbits. Fig. 2 depicts one orthographic view of the Lissajous and halo-type orbits used here. The halo-type orbit is significantly (approximately four times) larger in both the X and Y excursions from L1.
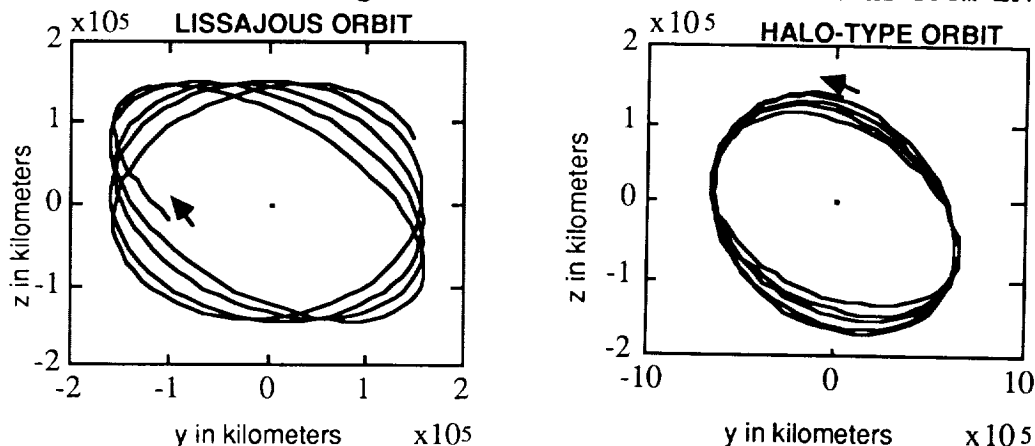
Fig. 2 Orthographic Depictions of the Reference Trajectories

Curve Fitting the Nominal Path

A numerical integration method developed by Howell and Pernicka[2] is used to generate a set of reference points at specified times for both position (three states) and velocity (three states), relative to the libration point of interest. The method computes numerical data in a reference frame that is centered at the libration point (in this case L1) and rotates with the primaries. However, the state estimation techniques and station-keeping algorithms used in this work require access to a continuous nominal path of acceptable accuracy. In one study, Pernicka[6] found that station-keeping costs for a libration point orbit were sensitive to the accuracy of the curve fit. A cubic spline interpolation routine was selected to model the reference trajectory here; the results of using other methods are summarized in the station-keeping section of this effort.

Examples of Experimental Design (DOE) Methods

DOE methods are used to purposefully change the most important inputs to a process in order to analyze the output. The inputs are coded and alternately set at predetermined values for each experimental run so that the design is orthogonal; the relative contribution of each input can thus be judged independently. The output of interest may be the mean response and its variation, with the ultimate goal being to hit an output target value and minimize the output variability. However, the results from the set of experimental runs also determine the estimated function that relates the inputs to the output(s). Experimental design methods are also used to reduce the required number of runs or screen out relatively unimportant input variables. When only three inputs at two different input levels are considered, a two-level, "full-factorial" design consisting of every possible combination of input factors would require $2^3 = 8$ total runs. This design allows the experimenter to obtain the full model with all possible interactions. However, if 7 inputs in a 2-level design were used, $2^7 = 128$ individual runs would be necessary. These 128 runs may be expensive in

terms of both time and money. As a result, fewer runs may certainly be desired. A full-factorial two-level design will include all input variables and their interactions in the output equation model, but this may not be required. If some interactions are known to be relatively unimportant, a fractional-factorial[7] design consisting of a fraction of the number of runs required in a full-factorial can be constructed.   For instance, for 3 inputs, a full-factorial would necessitate $2^3 = 8$ runs, while one type of fractional-factorial would require as few as 4 runs to determine the significance of main effects (modeling no interactions).

In a recent work by Garrett[8], several simple, yet educational, examples of the use of DOE are described. A similar example is included here: it is assumed that the area of a rectangle can be measured precisely, but the functional relationship between area and the length and width is not known. This example is truly hypothetical, but it can be used to illustrate simple DOE computations. The "design space" (where the computed model can be considered a good approximation to the true system) is defined by $1 \le$ width ≤ 2 meters and $1 \le$ length ≤ 3 meters. Here, "w" is used for width and "ℓ" for length. Runs are accomplished at the extreme values of the input variables, with $w = 1$ or 2 meters and $\ell = 1$ or 3 meters; however, first these measurements are generally coded. The data is coded by using the averages of both measurements and their ranges (highest value minus lowest).   With $R(\ell)$ = range of ℓ, $R(w)$ = range of w, $\overline{w}$ = average of the w extremes, and $\overline{\ell}$ = average of the ℓ extremes, the coded settings are w_c and ℓ_c:

$$w_c = 2\left(\frac{w-\overline{w}}{R(w)}\right), \qquad \ell_c = 2\left(\frac{\ell-\overline{\ell}}{R(\ell)}\right). \qquad (11)$$

When coded, the extreme values become +1 and -1 for each input, and these values are more simply denoted as "+" and "-", respectively. A balanced design with 4 runs then yields a design matrix of

RUN	w_c	ℓ_c	$(w_c)(\ell_c)$
1	-	-	+
2	-	+	-
3	+	-	-
4	+	+	+

The experiment is conducted using these high and low settings, and the measured areas of the rectangle (outputs) are 1, 3, 2, and 6 square meters for runs 1 through 4, respectively.   Schmidt and Launsby[7] discuss interesting hand computational methods to determine the output equation; however, simple least squares methods also provide identical results. The prediction equation for the output is assumed to be

$$\hat{a} = b_0 + b_1 w_c + b_2 \ell_c + b_3(w_c)(\ell_c) \qquad (12)$$

where $\hat{a}$ = estimated area and the coefficients are computed using a least squares method with

$$C = \begin{bmatrix} 1 & -1 & -1 & 1 \\ 1 & -1 & 1 & -1 \\ 1 & 1 & -1 & -1 \\ 1 & 1 & 1 & 1 \end{bmatrix} \text{ and } \overline{a} = \begin{bmatrix} 1 \\ 3 \\ 2 \\ 6 \end{bmatrix} \text{ in}$$

$$\overline{b} = (C^T C)^{-1} C^T \overline{a} = [b_0 \ b_1 \ b_2 \ b_3]^T. \qquad (13)$$

This method yields

$$\hat{a} = 3 + w_c + 1.5 \ell_c + .5 (w_c)(\ell_c). \qquad (14)$$

A similar method could be used to derive a prediction equation for the variance (or the natural logarithm of the standard deviation) of the output[7].   The

resulting model in Eq. (14) is normally checked by completing test (confirmation) runs at extreme values and at the midpoint of the design space. For this example, that could mean using values of +1 for both w_c and ℓ_c for an extreme run or 0 for both inputs for the midpoint run. Suppose a confirmation run was conducted at the extreme values and the resulting output was a = 6 meters. Using Eq. (14), the predicted output is

$$\hat{a} = 3 + 1 + 1.5(1) + .5(1)(1) = 6 \text{ meters.}$$

For a confirmation run at the midpoints, the measured answer is a = 3 meters. Using Eq. (14), the predicted output equation is

$$\hat{a} = 3 + 0 + 1.5(0) + .5(0)(0) = 3 \text{ meters.}$$

Hence, the confirmation runs verify the model; a significant disagreement would require further investigation. (In fact, this is the exact functional model--it's just coded.) When noise in the system exists, statistical tests are used to test confirmation. The coded Eq. (14) can now be converted to use uncoded inputs by using Eq. (11):

$$\hat{a} = 3 + (2)(w - 1.5) + (1.5)(2)\left(\frac{\ell-2}{2}\right) + (.5)(2)(w-1.5)(2)\left(\frac{\ell-2}{2}\right) = (w)(\ell).$$

This example was simplified because we obviously knew the actual output equation. In manufacturing or engineering problems, the relationship between inputs and outputs is only generally known, and DOE can be used to gain problem insight. In the next section, the orbit determination error analysis methods used in this effort are summarized. The following section describes the station-keeping methods derived for this work and summarizes the control-cost comparisons of halo and Lissajous orbits. Finally, modeling the inputs of the station-keeping routine in an experimental design is presented.

ORBIT DETERMINATION ERROR ANALYSIS

Complete, exact knowledge of the state of a spacecraft in orbit is generally not possible. Available measurements are usually some function of the state variables and are not precise. For instance, a spacecraft in a libration point trajectory in the Sun-Earth system may be tracked using range and range-rate measurements containing random errors. The spacecraft may be affected by forces inadequately represented in the dynamic model, and model parameters may be uncertain. By definition, the linearized system of equations used to model the nonlinear system is a further approximation. These sources of error make knowledge of the spacecraft state uncertain. Computation of the most likely current state of the spacecraft in the presence of measurement and model uncertainty is the focus of orbit determination.

Error analysis involves an investigation of the impact of various error sources on orbit determination. The outputs of this error analysis are the standard deviations of the states. These outputs could then be used to predict how an improvement in measurement accuracy, for instance, would lessen state uncertainty. One benefit of more accurate knowledge of the state might be a reduction in station-keeping costs. A mathematical procedure can be developed to combine all information about the spacecraft state, filtering this observed data based on the varying degrees of uncertainty, to obtain a "best estimate" of the state and an estimate of the resulting state variable uncertainties.

The measurement and dynamic models are first summarized, three error analysis methods are briefly discussed, and then results are summarized. The three error analysis methods used here are the Kalman filter, batch weighted least squares , and consider covariance analysis[5,11]. Each technique computes a covariance matrix

at a specified epoch, and the positive square roots of the diagonal entries are indicators of state uncertainty levels.

Measurement and Dynamic Models

The measurement and dynamic models used in the filter derivations are

$$\text{Measurements:} \quad \tilde{Z}_k = M_k \tilde{X}_k + \bar{V}_k, \tag{15}$$

$$\text{Dynamic Model:} \quad \tilde{X}_{k+1} = \Phi(t_{k+1}, t_k)\tilde{X}_k = \Phi(k+1,k)\tilde{X}_k, \tag{16}$$

where $\tilde{Z}_k$ is the measurement residual vector at time step k; $\tilde{X}_k$ is the residual state vector at time step k; M_k is the measurement matrix that is linearized about the nominal path; $\Phi(k+1,k)$ is the state transition matrix at time step k+1 relative to time step k; and $\bar{V}_k$ is the measurement noise vector with assumed statistics $E(\bar{V}_k)=\bar{0}$ and $E(\bar{V}_k\bar{V}_k^T)=V_k$, where "E" is the expectation operator, $\bar{0}$ is the zero vector, and V_k is the measurement noise covariance matrix. Range and range-rate measurements are assumed; the matrix, M, is then a time-varying matrix of dimension 2x6, evaluated along the nominal path.

Error Analysis Methods Used

Early work in this area was designed to compare the error levels obtained here to those found in other works and to determine error levels for use in follow-on station-keeping simulations. Three methods of orbit determination error analysis (using covariance analysis) were formulated: Kalman filter, batch weighted least squares, and consider covariance analysis. The results of Kalman and batch weighted least squares filters were virtually identical, as expected, but nonetheless helped to confirm the analysis. Both methods were formulated to compute state uncertainty after a predetermined number of tracking updates, simulating range and range-rate measurements with associated error statistics. Consider covariance analysis also uses a batch weighted least squares formulation but includes parameter uncertainty. Model parameters that were initially considered uncertain in this work were the planetary masses (through the dimensionless mass parameter μ), the locations of the tracking stations, and the solar reflectivity constant. In general, at the epoch of interest, the state uncertainty is considered the consequence of the accumulated uncertainties in the model, the parameters of interest, and the measurements[5,9-11].

Orbit Determination Error Analysis Results

A survey of input error levels used in similar error analysis studies serves as a valuable introduction. The values of these uncertainties may be used to compute diagonal entries of input covariance matrices for an error analysis, or, alternatively, may be used as error sources in a station-keeping simulation. Table 1 lists the input error levels assumed in several error analysis studies. The errors are denoted by the symbols generally used in the derivation sections of this work. The solar reflectivity constant is k; the tracking site location uncertainty is S and is input as an equal uncertainty level for each of the site coordinates x_s, y_s, z_s; range tracking is R; range-rate tracking is RR; and the uncertain mass parameters are μ_e for Earth, μ_s for the Sun, and μ_m for the Moon. The last column contains the uncertainty in dimensionless mass parameter μ that would be "equivalent" to the errors listed for the individual mass parameters. (Recall that $\mu = (\mu_e + \mu_m)/(\mu_s + \mu_e + \mu_m)$ for the three-body system of interest in this work.) The approximate value of $\sigma(\mu)$ (standard deviation of μ) is calculated

from extensive (10,000) Monte Carlo trials for each of these studies. An entry in Table 1 of "--" means the particular study did not indicate if an uncertainty of this type was used.

Table 1
SURVEY OF ERROR ANALYSIS INPUT ERRORS

STUDY	k	S (km)	R (km)	RR (m/sec)	ONE STANDARD DEVIATION ERRORS μ_e ($\leftarrow$ km^3/sec^2	μ_s $\rightarrow$)	μ_m	$\sigma(\mu)$ (x μ)
Mistretta[13]	15%	--	.010	.007	1.000	3.08×10^6	.0726	2.335×10^{-5}
Joyce[14]	10%	.002	.015	.002	.3986	1.327×10^4	.0490	1.411×10^{-7}
Efron[15,17]	10%	.002	.015	.002	.3986	1.327×10^4	.0490	1.411×10^{-7}
Rodriguez-Canabal[16]	--	.010	.015	.003	--	--	--	--
Longuski[17]	13%	.0003	.010	.001	.4903	4030.7	.0100	1.231×10^{-7}
This Work	13%	.010	.015	.003	.3986	1.327×10^4	.0490	1.411×10^{-7}

The error analysis conducted here assumes a 20-day tracking arc with 3 passes per day from 3 tracking sites. These assumptions closely match those of Joyce[14]. Using this tracking schedule and the R and RR measurement errors listed for this work in Table 1, the Kalman filter produces error levels presented in Table 2.

Table 2
RESULTS USING A KALMAN FILTER FOR ERROR ANALYSIS

ONE STANDARD DEVIATION LEVELS OF STATE ERRORS					
x (km)	y (km)	z (km)	$\dot{x}$ (mm/sec)	$\dot{y}$ (mm/sec)	$\dot{z}$ (mm/sec)
.550	1.600	4.450	.430	.775	2.250

The error levels listed in Table 2 are a result of a covariance analysis for the halo-type nominal path. The magnitudes of the error levels listed in Table 2 are, in fact, quite small; when additional error sources, such as mass parameter and station location uncertainties, are included in a consider covariance analysis, the resulting state error levels increase. The results in Table 3 are from a consider covariance analysis incorporating R and RR tracking, station location, and mass parameter uncertainties at the levels listed in Table 1 for this work.

Table 3
ERROR LEVELS PRODUCED FROM CONSIDER COVARIANCE ANALYSIS

| Coordinate | One Standard Deviation Levels | |
	Halo-Type Orbit	Lissajous Orbit
x (km)	1.46	1.25
y (km)	2.64	3.35
z (km)	4.81	3.19
$\dot{x}$ (mm/sec)	1.40	1.25
$\dot{y}$ (mm/sec)	1.85	1.41
$\dot{z}$ (mm/sec)	2.49	2.51

It certainly may be of great interest to compare the error levels found in this effort with the results of other investigations involving spacecraft in halo (or halo-type) orbits near the interior Sun-Earth libration point. Table 4 lists the results of four studies that do not include solar reflectivity as an error source and have small differences in the nominal paths and force models.

Table 4
COMPARISON OF ERROR ANALYSIS RESULTS FROM SEVERAL SOURCES

| Coordinate | One Standard Deviation Error Levels | | | |
	Rodriquez-Canabal[16]	Simó[18]	Simó[19]	This Work
x (km)	2.7	1.5	1.73	1.46
y (km)	3.9	2.5	2.24	2.64
z (km)	3.4	15.0	5.48	4.81
$\dot{x}$ (mm/sec)	2.4	1.0	1.41	1.40
$\dot{y}$ (mm/sec)	3.5	1.0	1.41	1.85
$\dot{z}$ (mm/sec)	1.3	3.0	2.45	2.49

The differences in error levels listed in Tables 3 and 4 may not be statistically significant; that is, station-keeping costs, determined through simulations using these error levels, may or may not differ statistically[5,12]. The results using one derived control scheme and the data in Table 3 are summarized in the next section.

STATION-KEEPING SIMULATIONS

For a collinear libration point orbit, a small deviation from the(unstable) nominal trajectory can lead to rather large drift from the path in a short time. In effect, a station-keeping algorithm must combat both the current drift from the path in addition to the exponential increase in the drift that is expected if no correction is implemented. Any delay in the control actuation may allow the drift to increase and thus compound the station-keeping problem. The goal of the station-keeping routine is then to keep the spacecraft "close enough" to the reference trajectory. The allowable deviations may depend on the simulation experience with a given control algorithm and on mission constraints, including the propellant cost that can be tolerated and the minimal time between control

inputs. When the spacecraft is "near" the nominal trajectory, it is reasonable to model the deviations from the reference path using a linear analysis.

Derivation of Method

For the linear control scheme developed here, the state transition matrix is partioned into four 3x3 submatrices as

$$\Phi(t_k, t_\emptyset) = \begin{bmatrix} A_{k\emptyset} & B_{k\emptyset} \\ C_{k\emptyset} & D_{k\emptyset} \end{bmatrix} = \begin{bmatrix} A_k & B_k \\ C_k & D_k \end{bmatrix} \tag{17}$$

A $\overline{\Delta v}$ input (a 3x1 vector), with magnitude denoted as Δv, is assumed to be added at a time $t_\emptyset$. The $\overline{\Delta v}$ (delta-velocity) is added to the initial velocity states in the numerical integration routine in order to change the deviation of the spacecraft from the nominal path at some future time. In this derivation, $\overline{p}_k$ is the position deviation (a 3x1 vector) and $\overline{v}_k$ is the velocity deviation (a 3x1 vector) of the spacecraft from the nominal path at time t_k, with $k = 1, 2, 3$ and 4. If $\overline{v}_\emptyset$ is the residual velocity (a 3x1 vector) and $\overline{p}_\emptyset$ is the residual position (a 3x1 vector) relative to the nominal path at time $t_\emptyset$, then a $\overline{\Delta v}$ input at $t_\emptyset$ could be used to predict $\overline{p}_k$ for $k = 1, 2, 3$ and 4. For instance, when the initial position $\tilde{X}_\emptyset$ includes an initial velocity perturbation $\overline{v}_\emptyset$, a delta velocity $\overline{\Delta v}$, and an initial position perturbation $\overline{p}_\emptyset$, the state propagation equation results in

$$\tilde{X}_k = \begin{bmatrix} \overline{p}_k \\ \overline{v}_k \end{bmatrix} = \Phi(t_k, t_\emptyset) \tilde{X}_\emptyset = \Phi(t_k, t_\emptyset) \begin{bmatrix} \overline{p}_\emptyset \\ \overline{v}_\emptyset + \overline{\Delta v} \end{bmatrix}. \tag{18}$$

The cost function used to derive this control scheme is

$$J(\overline{\Delta v}) = \overline{\Delta v}^T Q \overline{\Delta v} + \overline{p}_1^T R \overline{p}_1 + \overline{v}_1^T R_v \overline{v}_1 + \overline{p}_2^T S \overline{p}_2 + \overline{v}_2^T S_v \overline{v}_2$$

$$+ \overline{p}_3^T T \overline{p}_3 + \overline{v}_3^T T_v \overline{v}_3 + \overline{p}_4^T U \overline{p}_4 + \overline{v}_4^T U_v \overline{v}_4, \tag{19}$$

where Q is a positive definite weighting matrix and R, R_v, S, S_v, T, T_v, U, and U_v are positive semidefinite weighting matrices. The cost function can be written in terms of $\overline{\Delta v}$ by using substitutions for $\overline{p}_k$ and $\overline{v}_k$, with $k = 1, 2, 3$, and 4, derived from Eqs. (17) and (18). The minimum is then $\overline{\Delta v} =$

$$-[Q + B_1^T R B_1 + B_2^T S B_2 + B_3^T T B_3 + B_4^T U B_4 + D_1^T R_v D_1 + D_2^T S_v D_2 + D_3^T T_v D_3 + D_4^T U_v D_4]^{-1}$$

$$\times[(B_1^T R B_1 + B_2^T S B_2 + B_3^T T B_3 + B_4^T T B_4 + D_1^T R_v D_1 + D_2^T S_v D_2 + D_3^T T_v D_3 + D_4^T U_v D_4)\overline{v}_\emptyset +$$

$$(B_1^T R A_1 + B_2^T S A_2 + B_3^T T A_3 + B_4^T U A_4 + D_1^T R_v C_1 + D_2^T S_v C_2 + D_3^T T_v C_3 + D_4^T U_v C_4)\overline{p}_\emptyset].$$

A simpler version of this controller can be used by setting, for instance, the weighting matrices U and U_v equal to the 3x3 zero matrix. This modified controller is the one used in the following section.

Comparison of Halo-Type and Lissajous Orbits

The cost of maintaining the spacecraft in orbit for 2 years is selected as the comparison value. For each simulation run, tracking updates, with assumed error levels listed in Table 3, are input every 20 days. Solar radiation pressure uncertainty is also input as an error source with magnitude listed in Table 1. The errors are modeled as zero-mean Gaussian random variables. Each simulation of the station-keeping algorithm will be a random trial with the random variable of

interest being the total magnitude of the station-keeping costs (ΔV_T) for the 2-year simulation. A sequence of 30 Monte Carlo station-keeping simulations produces a random sample of 30 random variables. Sample statistics, such as means and standard deviations, can then be calculated, and statistical tests can be conducted to compare the mean control costs for halo-type and Lissajous orbits[5,12]. Table 5 contains the results of one set of simulations using 30 Monte Carlo trials for each type of orbit.

Table 5
COMPARISON OF STATION-KEEPING COSTS

Lissajous Orbit			Halo-Type Orbit		
Avg ΔV_T (m/s)	Std Dev (m/s)	Range (m/s)	Avg ΔV_T (m/s)	Std Dev (m/s)	Range (m/s)
.8450	.1603	.57 - 1.15	.8124	.1233	.62 - 1.08

Statistical hypothesis tests conclude that the 2-year mean control cost, using the two nominal paths and this particular controller, are equal. The conclusion of equal station-keeping costs for all nominal paths near this libration point and any control scheme cannot be drawn from this work.

Comparison of Station-Keeping Costs for Different Curve Fitting Options

Various curve fitting methods have been developed to model the nominal paths. While cubic splines are used here, least squares curve fits for a trigonometric series and linear interpolation routines have also been tested. The data in Table 6 summarizes efforts to date. The curve fits are indexed by the number of terms included in the Fourier series. The cubic spline and linear interpolation schemes are indexed by the time between points.

Table 6
COMPARISON OF CONTROL COSTS BY CURVE FITTING TECHNIQUES

Cubic Spline	Average 2-Year Cost (meters/sec)
Days between points = 3, 6, 9	1.234, 1.801, 10.324
Fourier Series	
Terms Used = 28, 91, 121, 161	9.577, 8.147, 1.419, 1.414
Linear Interpolation	
Days between points = .5, 1, 2, 6	1.290, 1.307, 1.333, 38.604

EXPERIMENTAL DESIGN RESULTS

The process of interest here is station-keeping for a 2-year halo-type Lagrange point orbit in the Sun-Earth+Moon elliptic restricted three-body problem. The input variables include tracking errors (track), solar radiation pressure (SRP) and mass ratio (mass) uncertainties, orbit injection errors (inject), and thruster (thrust) errors. The outputs of interest are the 2-year control cost (ΔV_t) and its variance. Other inputs could be considered, and additional outputs, such as the number of ΔV inputs required or the average separation time between control inputs, could also be evaluated in future efforts. The relationship of the inputs, the process, and the outputs is depicted in Fig. 3.

TRACKING ERRORS (TRACK)

SOLAR RADIATION PRESSURE UNCERTAINTY (SRP)

MASS PARAMETER UNCERTAINTY (MASS)

STATION-KEEPING

ORBIT INJECTION ERRORS (INJECT)

THRUST INPUT ERRORS (THRUST)

2-YEAR CONTROL COST (ΔV_t) AND ITS VARIANCE ($S^2(\Delta V_t)$)
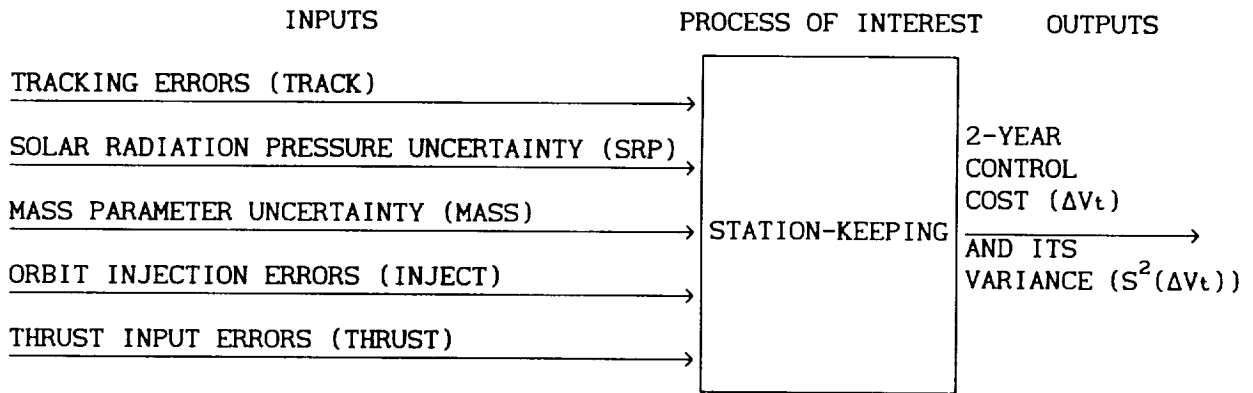
Fig. 3 Process of Interest

For this analysis, a fractional factorial two-way design was selected in order to limit the total number of runs. A fractional factorial 2^{5-1} design[7] allows use of only 16 runs to pick out contributions of the 5 main inputs and 10 two-way interactions. The design matrix, with only the main effects listed, is depicted in Fig. 4.

RUN	INPUT VARIABLES
	a	b	c	d	e=abcd
	TRACK	THRUST	SOLAR	MASS	INJECT
1	−	−	−	−	+
2	−	−	−	+	−
3	−	−	+	−	−
4	−	−	+	+	+
5	−	+	−	−	−
6	−	+	−	+	+
7	−	+	+	−	+
8	−	+	+	+	−
9	+	−	−	−	−
10	+	−	−	+	+
11	+	−	+	−	+
12	+	−	+	+	−
13	+	+	−	−	+
14	+	+	−	+	−
15	+	+	+	−	−
16	+	+	+	+	+

Fig. 4 Design Matrix

A full factorial would enable analysis of 5 main effects, 10 two-way interactions, 10 three-way interactions, 5 four-way interactions, and 1 five-way interactions. Generally, interactions above two-way are not significant contributors to a model[7]. The modeled interactions not depicted in Fig. 4 are ab, ac, ad, ae, bc, bd, be, cd, ce, and de. Note also that the main effect "inject" is aliased[7] with the abcd four-way interaction. The full factorial two-level design would allow analysis of all possible interactions that could affect the output. It would not allow curvature analysis (quadratic effects), but these could be analyzed using a sequential central composite design approach[7]. Investigation of quadratic effects would be necessary only if confirmation runs indicate poor agreement at the midpoint of the design space. The design space is determined by the extreme values selected for each input. That is, the low and high settings for each input determine the region over which the approximate

output equations are defined. A large range for an input will also have a great bearing over whether it will be found significant. For this design, the low and high settings for each input are depicted in Table 7.

Table 7
LISTING OF DESIGN INPUTS AND SETTINGS

Input	Settings	
	Low (−)	High (+)
Track		
x	1 KM	3 KM
y	2 KM	10 KM
z	4 KM	15 KM
x dot	.0010 m/sec	.008 m/sec
y dot	.0015 m/sec	.010 m/sec
z dot	.0020 m/sec	.015 m/sec
Solar	2.5%	15%
Mass	1.231×10^{-7}	5.000×10^{-6}
Inject		
Each position coordinate	1.5 KM	50 KM
Each velocity coordinate	.001 m/sec	.05 m/sec
Thrust (each direction)	2.5%	10%

These input settings are representative of those used in other orbit determination error analysis and station-keeping studies. (See Tables 1 and 4.) The resulting output equations for the predicted ΔV (here denoted as $\Delta \hat{V}$) and natural logarithm of the output variance (denoted as $\ln(\hat{S})$) are

$$\Delta \hat{V} = 2.9348 + 1.3627 \text{ Track} + .2953 \text{ Thrust} + .0263 \text{ Solar} + .0028 \text{ Mass}$$
$$- .0904 \text{ Track-Thrust} - .0605 \text{ Track-Solar} - .0215 \text{ Thrust-Solar}$$
$$- .0103 \text{ Track-Mass} - .0065 \text{ Thrust-Mass} + .0395 \text{ Solar-Mass} +$$
$$- .0090 \text{ Solar-Inject} + .0551 \text{ Thrust-Inject} + .0094 \text{ Mass-Inject}$$
$$- .0299 \text{ Track-Inject} + .05 \text{ Inject}, \tag{20}$$

$$\ln(\hat{S}) = 0.2027 + 0.5948 \text{ Track} + .2334 \text{ Thrust} + .1221 \text{ Solar} + .0567 \text{ Mass}$$
$$- .1614 \text{ Track-Thrust} - .0959 \text{ Track-Solar} + .0093 \text{ Thrust-Solar}$$
$$+ .0517 \text{ Track-Mass} + .0074 \text{ Thrust-Mass} - .0297 \text{ Solar-Mass}$$
$$- .0339 \text{ Solar-Inject} - .0394 \text{ Thrust-Inject}$$
$$+ .0238 \text{ Mass-Inject} - .0127 \text{ Track-Inject} + .0292 \text{ Inject}. \tag{21}$$

Additional experimental runs showed that the output model confirmed at the design midpoint and at both extremes. Often, this sort of model is used to determine optimal input settings: in order to minimize both ΔV and $\ln(S)$ in Eqs. (20) and (21), all inputs should be set at the minimum settings. However, a more realistic

407

use of these equations is for sensitivity analysis: the size of the coefficient of each input is a measure of that variable's influence on the output. These results show that tracking and thrust input errors are responsible for a large portion of the control cost. By reducing these two errors to their minimum, nominal savings on the order of 50% are predicted.

CONCLUSION

With the continuing importance of solar research, the use of libration point orbits between the Sun and the Earth is both an interesting and valuable area of effort. The need for orbit determination error analysis in conjunction with pre-mission station-keeping simulations was the original driving force behind this work. The results of three error analysis methods were compared with other similar libration point studies. The outputs of the error analysis were the six states' standard deviations. These error levels could then, in turn, be used as error sources in Monte Carlo simulations of derived station-keeping routines. With nominal paths that could be constructed as nearly periodic halo-type, or distinctly quasi-periodic and smaller Lissajous trajectories, the error analysis and station-keeping results may differ by the type of orbit selected. Statistical tests for the equality of the average 2-year control costs using halo-type and Lissajous paths strongly suggest that there is no difference in mean station-keeping costs. It should, however, be noted that the results are presented for only one particular control algorithm and for two specific nominal trajectories. Experimental design methods are then used to determine the approximate functional relationship between the input uncertainties and the output 2-year control cost. This type of functional relationship seems more useful than a series of tabular entries of control costs, each corresponding to a different set of input error levels.

REFERENCES

1.   R.W. Farquhar, "A Halo-Orbit Lunar Station," *Astronautics and Aeronautics*, June 1972, pp. 59-63

2.   K.C. Howell and H.J. Pernicka, "Numerical Determination of Lissajous Trajectories in the Restricted Three-Body Problem," *Celestial Mechanics*, Vol. 41, 1988, pp. 107-124

3.   S.C. Gordon, "Representing the Nominal Path for an Interior Libration Point Orbit in the Sun-Earth+Moon Elliptic Restricted Three-Body Problem," USAFA-TR-91-11, United States Air Force Academy, Colorado, Sept. 7, 1991

4.   J.L. Bell, "The Impact of Solar Radiation Pressure on Sun-Earth L1 Libration Point Orbits," M.S. Thesis, School of Aeronautics and Astronautics, Purdue University, West Lafayette, Indiana, Aug. 1991

5.   S.C. Gordon, "Orbit Determination Error Analysis and Station-Keeping for Libration Point Trajectories," PhD Dissertation, School of Aeronautics and Astronautics, Purdue University, West Lafayette, Indiana, Dec. 1991

6.   H.J. Pernicka, "The Numerical Determination of Nominal Libration Point Trajectories and Developement of a Station-Keeping Strategy," PhD Dissertation, School of Aeronautics and Astronautics, Purdue University, West Lafayette, Indiana, May 1990

7.   S.R. Schmidt and R.G. Launsby, Understanding Industrial Designed Experiments, CQG Printing, Longmont, Colorado, 2nd Ed, 1992

8. D.W. Garrett, "Experimental Design: Explanation by Example," DFMS TR 91-2, United States Air Force Academy, Colorado, Feb. 1991

9. B.D. Tapley and V. Szebehely, Editors, *Recent Advances in Dynamical Astronomy*, B.D. Tapley, "Statistical Orbit Determination Theory," D. Reidel, Dordrecht-Holland, 1988, pp. 396-425

10. B.D. Tapley, G. H. Born, and B. E. Schutz, *Satellite Orbit Determination*, University of Texas at Austin, June 1985

11. S.C. Gordon, "Orbit Determination Error Analysis for an Interior Libration Point Orbit in the Sun-Earth+Moon Elliptic Restricted Three-Body Problem," USAFA-TR-91-12, United States Air Force Academy, Colorado, Sept. 7, 1991

12. S.C. Gordon, "Comparison of Station-Keeping Algorithms for an Interior Libration Point Orbit in the Sun-Earth+Moon Elliptic Restricted Three-Body Problem," USAFA-TR-91-12, United States Air Force Academy, Colorado, Oct. 10, 1991

13. G.D. Mistretta, "Preliminary Considerations for an ISEE-C Least Squares Orbit Determination Strategy," Goddard Space Flight Center, Report X-580-76-251, Nov. 1976

14. J.B. Joyce, S.J. Leszkiewicz, and A.F. Schanzle, "Trajectory Determination Support and Analysis for ISEE-3 from Halo Orbit to Escape from Earth/Moon System," AAS Paper 79-128

15. L. Efron, D.K. Yeomans, and A.F. Schanzle, "ISEE/ICE Navigation Analysis," *The Journal of the Astronautical Sciences*, Vol. 33, Number 3, July-Sept. 1985, pp. 301-323

16. J. Rodriguez-Canabal, "SOHO Mission Analysis," ESOC Mission Analysis Office, June 1984

17. Personal Communications with J.M. Longuski (School of Aeronautics and Astronautics, Purdue University, West Lafayette, Indiana) and with L. Efron, J. Campell, and M. Standish (Jet Propulsion Laboratory, California Institute of Technology, Pasadena, California), Aug. 29, 1991

18. C. Simó, G. Gómez, J. Llibre, and R. Martínez, "Station Keeping of a Quasiperiodic Halo Orbit Using Invariant Manifolds," Proceedings of the Second International Symposium on Spacecraft Flight Dynamics, Darmstadt, Federal Republic of Germany, 20-23 Oct. 1986

19. G. Simó, G. Gómez, J. Llibre, R. Martínez, and J. Rodriguez, "On the Optimal Station Keeping Control of Halo Orbits," *Acta Astronautica*, Vol. 15, No. 6/7, 1987, pp. 391-397